Research Paper

Liver segment imaging using monocyte sequestration: a potential tool for fluorescence-guided liver surgery

Baifeng Qian[1], Daisuke Kyuno[1, 2], Michael Schäfer[1], Wolfgang Gross[1], Arianeb Mehrabi[1], Eduard Ryschich[1✉]

1. Department of General, Visceral and Transplantation Surgery, University Hospital Heidelberg, Heidelberg, Germany.
2. Department of Surgery, Surgical Oncology and Science, Sapporo Medical University, Sapporo, Japan.

✉ Corresponding author: Eduard Ryschich, University Hospital Heidelberg, Department of General Surgery, Im Neuenheimer Feld 365, 69120 Heidelberg, Germany. Phone: +49-6221-56-6110; Fax: +49-6221-56-5199; E-mail: eduard.ryschich@med.uni-heidelberg.de

Abstract

Background: The accurate determination of liver segment anatomy is essential to perform liver resection without complications and to ensure long-term outcomes after this operation. There are several perioperative methods for segment identification and surgical navigation, such as intraoperative ultrasound, indigo carmine and near-infrared imaging with indocyanine green. The present study experimentally analyzed the usefulness of monocyte sequestration for liver segment labeling and imaging.

Methods: Human monocytes were isolated from peripheral blood and directly or indirectly labeled with calcein or IRDye 800CW. Potential toxicity, labeling stability, and adhesion to ICAM-1 were analyzed *in vitro*. Monocyte sequestration in the liver microvasculature and liver segment labeling and boundary demarcation were studied using isolated mouse and pig liver perfusion and via intraportal injection in mouse liver tumor models.

Results: The highest monocyte labeling efficiency was achieved using direct labeling with IRDye 800CW. Labeling was stable and did not influence cell viability. The labeled monocytes were highly sequestrated in the liver microvasculature, both after *ex vivo* perfusion and after injection *in vivo*, resulting in excellent labeling of selected liver segments and strong segment boundary demarcation. In contrast to results to a normal liver, monocyte sequestration was very low in tumor-associated blood vessels.

Conclusions: The present experimental study shows that sequestration of labeled monocytes after superselective application demarcates the selected liver segment. These results illustrate potential of this technique for surgical navigation during liver surgery.

Key words: Intraoperative navigation; IRDye 800CW; intravascular sequestration

Introduction

Liver resection is used for the surgical treatment of liver tumor, such as hepatocellular cancer, and metastases of gastroenterological cancers [1, 2]. To perform this operation without complications and to ensure long-term outcomes, the accurate determination of liver segment anatomy is necessary [3, 4]. There are several perioperative methods for segment identification and surgical navigation. Intraoperative ultrasound [5, 6] is widely used for intraoperative navigation in clinical liver surgery. The use of indigo carmine [7] and near-infrared (NIR) imaging [8, 9] to label and visualize liver segments has been studied intensively in recent years. Indigo carmine use is quite limited because the segment demarcation is not ideal and the color disappears 10 min after injection [10]. At the current time, there is a single NIR-fluorescent dye, indocyanine green (ICG) which is approved by US Food and Drug

Administration. Clinical NIR imaging is mainly based on the superselective injection of ICG into the segmental branch of the portal vein using ultrasound, but anatomic segment can also be visualized using systemic ICG injection [11]. Recent studies demonstrated practicability of different application regimens of ICG [10, 12-14]. Although ICG is effective for image-guided liver surgery, it does not always provide a sufficient segment contrast and temporal stability because the dye disappears gradually after injection [13, 15]. ICG injection is only possible if the surgeon is well trained in ultrasound techniques and if ultrasound can be used. For example, it may be difficult to use ultrasound in some cases of repeated liver resection. ICG is also contradicted in patients with iodine allergy although the rate of such adverse reaction is usually very low [16]. Alternative technologies that result in better labeling and in stronger demarcation of segment boundaries may improve intraoperative navigation in liver surgery, at least in cases in which ICG labeling is not feasible.

Circulating leukocytes in the blood can leave the vasculature and migrate into tissues, where they function as immune cells. Although the diameter of some types of leukocytes, such as monocytes and neutrophils, is greater than the diameter of capillaries, leukocytes freely "squeeze" through the smallest microvascular blood vessels [17, 18]. Pro-inflammatory signals induce the interactions of leukocytes with endothelial cells and promote subsequent leukocyte extravasation. There are two types of leukocyte-endothelium interactions. The first type is leukocyte adhesion to the venular endothelium, which precedes leukocyte extravasation into the site of inflammation [19, 20]. The second type is leukocyte capture in capillaries, also known as leukocyte sequestration [21]. The physiological role of leukocyte sequestration is poorly understood, although this type of leukocyte adhesion to the endothelium is not attributed to leukocyte extravasation [22]. Both interactions are mediated by similar molecular mechanisms i.e. by interactions between specific adhesion molecules on leukocytes and on endothelial cells, although different adhesion molecules are involved in the different interactions [21, 23].

The present study experimentally analyzed whether leukocyte sequestration could be exploited for liver segment labeling and imaging. Monocytes were used because they can be isolated in sufficient number from peripheral blood samples and because they have a greater diameter than most other leukocyte types.

Materials and methods

Monocyte isolation

Human peripheral blood mononuclear cells (PBMCs) were isolated by density gradient centrifugation from the buffy coats of healthy donors using 1.077 g/mL Biocoll (Biochrom, Berlin, Germany). Monocytes were isolated from PBMCs using the Human CD14 Positive Selection Kit (BioLegend, San Diego, CA, USA) by positively immunomagnetic selection according to the manufacturer's instructions. This yielded a population of CD14+ cells that was at least a 90% pure as assessed by fluorescence-activated cell sorter analysis (Figure S1A).

Efficiency of monocyte labeling with IRDye 800CW

We determined the efficiency of different monocytes labeling strategies i.e. one-step versus two-step antibody-based labeling versus direct labeling. Antibodies were conjugated to IRDye 800CW using its N-Hydroxysuccinimide (NHS) ester according to the manufacturer's instructions (Licor, Lincoln, NE, USA). IRDye 800CW-conjugated anti-human CD14 mAb (clone M5E2, BioLegend) was used for one-step antibody-based labeling. For two-step labeling, monocytes were labeled with specified antibodies and isotypes and subsequently with IRDye 800CW-conjugated secondary antibody (Table 1). For direct labeling, monocytes were co-incubated with different concentrations of IRDye 800CW NHS ester. The fluorescence of cell suspensions was then measured using standard parameters of Odyssey CLx imager (Laser: 800 nm; intensity: L2; distance, 1 mm; resolution: 169 μm). The labeling efficiency was calculated and expressed as the doses per million cells. The time-course of changes in the fluorescence signal was analyzed to study the labeling stability.

Monocyte adhesion to ICAM-1

Microfluidic chambers (μ-Slide VI 0.4, Ibidi, Martinsried, Germany) were incubated with mouse ICAM-1 (4 μg/mL, Sino Biological, Beijing, China) for 2 h to coat the chambers were then blocked for 1 h with 10% bovine serum albumin (Roth, Karlsruhe, Germany) solution. Monocytes (100,000/chamber) were allowed to adhere to the surface for 5 min. Non-adherent cells were removed by perfusion with phosphate-buffered saline (PBS) at 1 N/m² shear stress using a microperfusion pump (WPI, Sarasota, FL, USA). The number of adhered monocytes was counted using microscopy (AxioObserver Z1, Zeiss, Jena, Germany) and expressed per square millimeter.

Table 1. The list of antibodies used in two-step labeling

	Primary antibody				Secondary antibody (IRDye800CW-conjugated Goat anti-Mouse IgG)
	Antigen	Clone	Isotype	Dose (μg/10^{6}cells)	Dose (μg/mL)
a	CD14	M5E2	mouse IgG2a, κ	2	5
b	CD16	3G8	mouse IgG1, κ	2	5
c	CD64	10.1	mouse IgG1, κ	0.5	5
d	CD14 / CD16/ CD64	M5E2 / 3G8/ 10.1	mouse IgG2a, κ / mouse IgG1, κ/ mouse IgG1, κ	2 / 2/ 0.5	5
e	Isotype 1	MOPC-21		2	5
f	Isotype 2	MOPC-173		2	5
g	Isotype 1/ Isotype 2	MOPC-21/ MOPC-173		2 / 2	5
h	no				5
i	no				no

The primary antibodies were purchased from BioLegend and the secondary antibody was purchased from Licor.

Isolated liver perfusion in mice

The animal experiments were performed in accordance with international rules and were approved by the local animal care committee (Regierungspräsidium Karlsruhe). The livers of C57BL/6 mice (Charles River, Sulzfeld, Germany) were isolated and prepared for perfusion through portal vein as described previously [24]. Monocytes were labeled with calcein-AM (4 μg/mL, Sigma-Aldrich, Munich, Germany) for 15 min at room temperature. After two washes with PBS, the monocytes were filtered through a 35-μm cell strainer (Corning, Reynosa, Tamaulipas, Mexico), and their concentration was adjusted to 1×10^6 cells/mL in 0.9% sodium chloride solution for liver perfusion. To label the microvascular system, 800 ng of R-phycoerythrin (RPE)-conjugated ME-9F1 mAb (Biolegend) was perfused in each liver. Next, the livers were perfused using intermittent perfusion/effluent collection cycles at a 1 mL/min flow rate, with 1×10^6 cells in 1 mL of solution perfused every minute. Monocytes in the effluent were counted, and monocyte sequestration was analyzed using a fluorescence microscopy system (AxioObserver Z1, Zeiss) equipped with a monochromatic light source (488 nm, 555 nm, Colibri, Zeiss) and control software (AxioVision 2012, Zeiss).

In other experiments that used isolated mouse liver perfusion, the left branch of the portal vein was clamped, and IRDye 800CW-conjugated monocytes were perfused at a rate of 0.25 or 1 mL/min. After perfusion, the livers were analyzed using an NIR imager as described above. The whole liver and the perfused lobes were weighed, and the mean fluorescence intensity (MFI) of the perfused and non-perfused segments was compared.

Isolated liver perfusion in pigs

Male pigs (22–27 kg) (Bräunling, Nussloch, Germany) were pre-medicated using intramuscular injection of azaperone (8 mg/kg, Elanco, Bad Homburg, Germany), ketamine (12–15 mg/kg, Bremer Pharma, Warburg, Germany) and midazolam (500 μg/kg, Hameln pharma plus, Hameln, Germany), and then sacrificed using intravenous injection of potassium chloride (2 mmol/kg, B. Braun Melsungen, Melsungen, Germany). The livers were isolated immediately and the portal vein and the hepatic artery were perfused using oxygenated Krebs-Henseleit buffer [25].

After blood removal, a medical catheter (∅ 0.61 mm) was inserted and moved into the selected segmental artery. IRDye 800CW-conjugated monocytes were injected using a flow rate of 1 mL/min. After perfusion, the liver was imaged using an NIR imager as described above. The MFI of the perfused and non-perfused segments was analyzed.

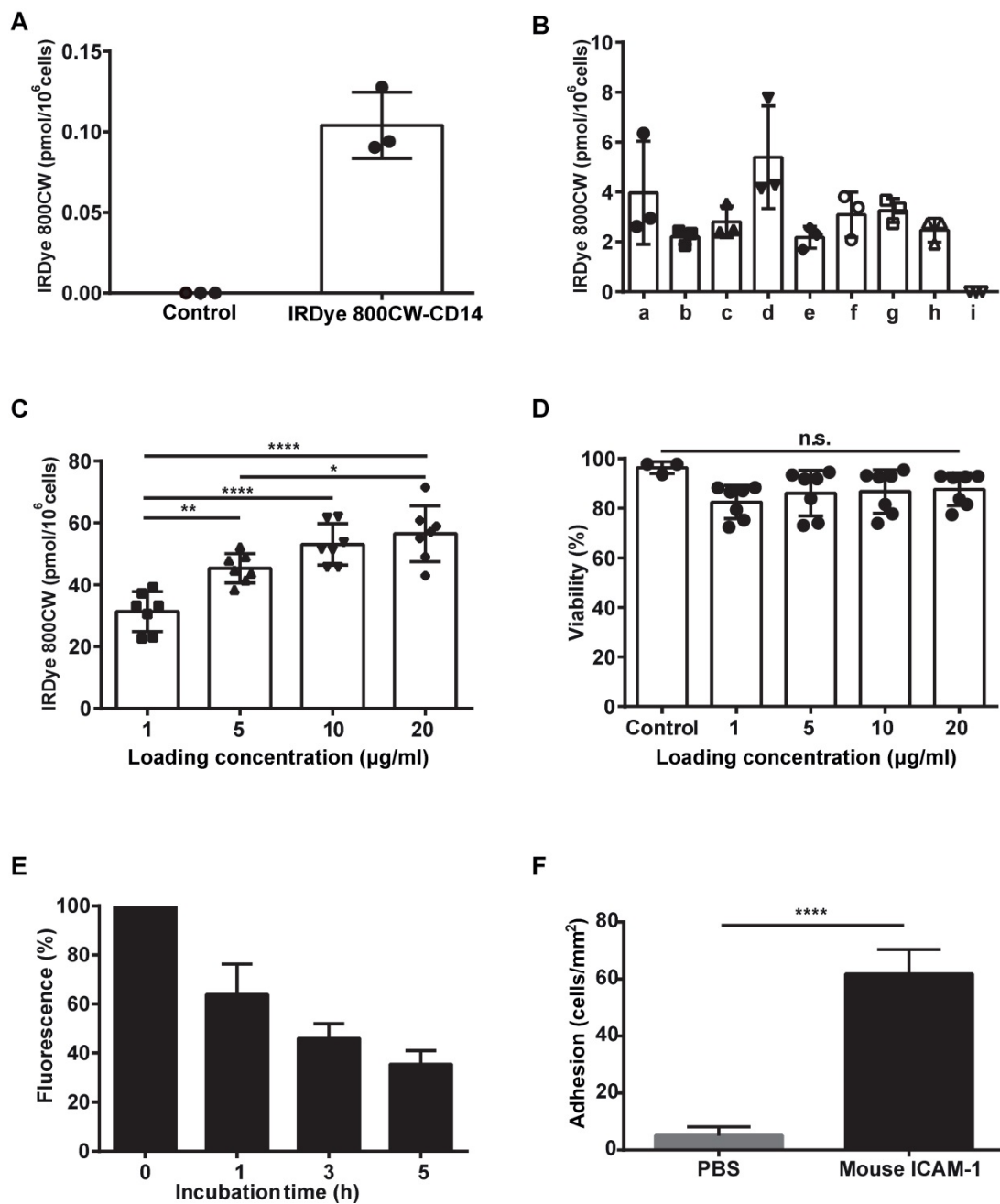## Monocyte injection in tumor models

Hepatic tumors were induced in male C57BL/6 mice (10–14 weeks) using intrahepatic inoculation of Panc02 (pancreatic cancer) cells or Hep55.1C (hepatoma) cells ($1–1.6 \times 10^6$/inoculation). Mice were anaesthetized with isoflurane 12–14 days after inoculation. The monocytes were treated with calcein-AM for perfusion, and RPE-conjugated ME-9F1 mAb (Biolegend) was used to label the microvascular system. Selective hepatic artery injection using a 34G needle (Hamilton, Bonaduz, Switzerland) was used for monocyte injection as described previously [24]. Mice were sacrificed 5–10 minutes after injection, and their organs were removed and imaged using fluorescence microscopy (AxioObserver Z1, Zeiss).

Selective portal vein perfusion was performed to assess the demarcation of selected liver segments and tumor localization. The left branch of the portal vein, which did not support the tumor-bearing segment, was clamped, and 750,000 IRDye 800CW-labeled monocytes or a fluorescence equivalent of ICG (Figure S1B) were injected into the right branch of the portal

vein using a microsyringe (Hamilton) and a 30G needle (BD, Drogheda, Ireland). The clamp was removed immediately after injection. The waiting time of 5 min was taken to allow the recovery of blood circulation. The mice were sacrificed, and then the organs were removed and imaged using Odyssey CLx as described above.

Statistical analysis

Statistical analysis was performed using SPSS statistics software (IBM, Armonk, NY, USA). Data are reported as the mean ± standard deviation (SD). To analyze differences between the groups, a t-test, one-way ANOVA followed by Bonferroni correction test or Kruskal-Wallis test and mixed ANOVA followed by Bonferroni correction test were used. $P < 0.05$ was considered significant.
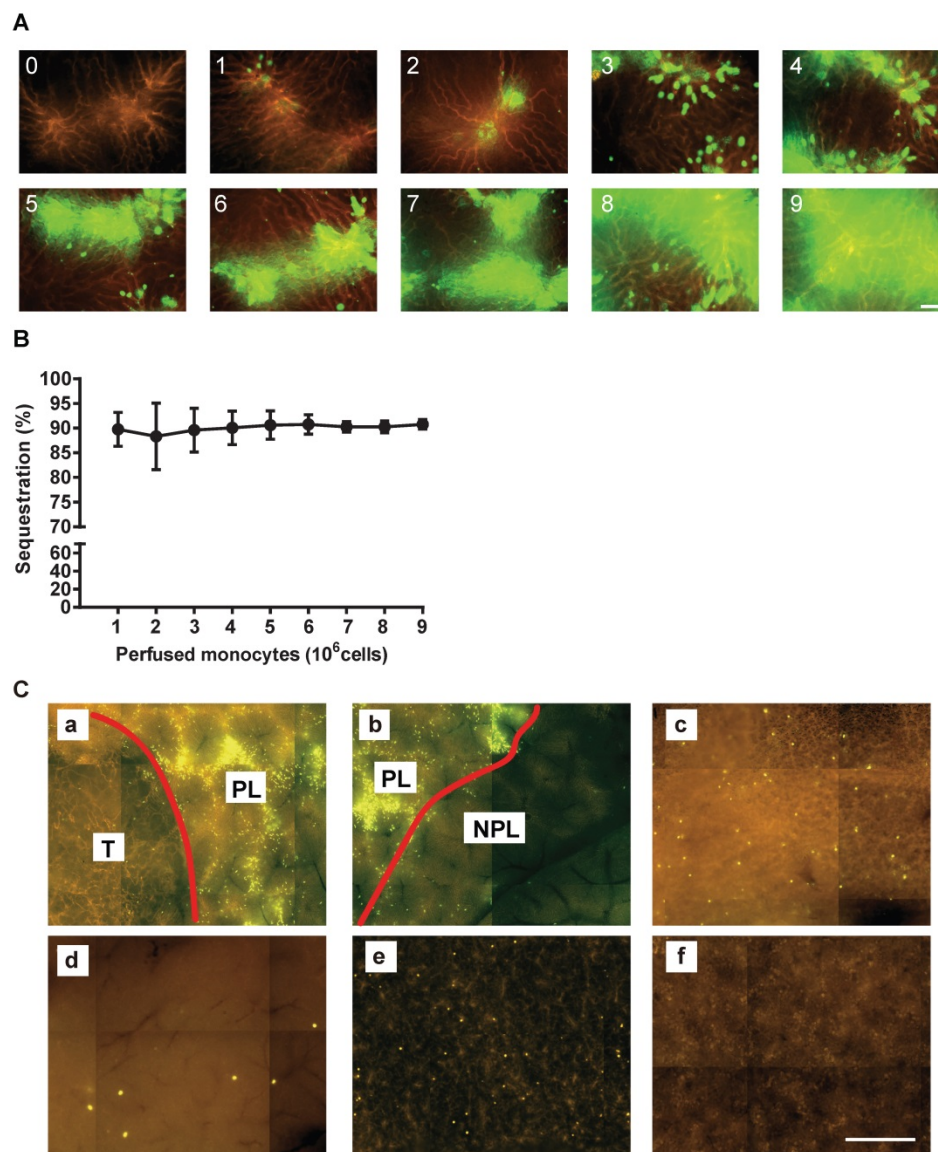
Figure 1. Labeling monocytes with IRDye 800CW: dye stability and the adhesion o mICAM-1. (A) Labeling efficiency of monocytes using one-step IRDye800CW-conjugated anti-CD14 mAb. (B) Two-step labeling using IRDye800-conjugated secondary antibody to the following primary mAbs: a, anti-CD14; b, anti-CD16; c, anti-CD64; d, anti-CD14, anti-CD16 and anti-CD64; e, isotype 1 (mouse IgG2a); f, isotype 2 (mouse IgG1); g, isotypes 1 and 2; h, secondary Ab only; i, PBS (negative control). (C) Direct conjugation using the indicated different concentrations of the IRDye 800CW NHS ester. (D) Monocyte viability. (E) Labeling stability over time. (F) Monocyte adhesion to ICAM-1. Data are presented as means ± SDs for three or more independent experiments. One-way ANOVA followed by the Bonferroni correction test was used for the analysis in (C), one-way ANOVA followed by the Kruskal-Wallis test was used for the analysis in (D), and a t-test was used for the analysis in (F). n.s. no significant difference; *P < 0.05; **P < 0.01; ****P < 0.001.

Results

Efficiency, stability, and potential toxicity of IRDye 800CW labeling of monocytes and their adhesion to ICAM-1 *in vitro*

The contrast observed in liver segment labeling *in vivo* is expected to correlate with monocyte labeling intensity. We thus compared one-step and, two-step antibody labeling and direct labeling with IRDye 800CW to determine which method yielded the most fluorescent labelling. Although monocyte-specific antibodies showed substantial cell labeling using both the one-step and the two-step labeling methods (Figure 1A-B), incubation with the IRDye 800CW NHS ester resulted in the highest IRDye 800CW dose accumulation, which was approximately 10-fold more intense than the highest level achieved using antibody labeling (Figure 1C). A viability assay demonstrated that IRDye 800CW did not have any toxic effects on monocytes *in vitro* (Figure 1D). Furthermore, measurement of the fluorescence signal over time showed that monocyte IRDye 800CW labeling decreased slowly, with a half-life of 2.26 h (Figure 1E). Using a microfluidic setup, we found that monocytes effectively adhered to mouse ICAM-1 but showed almost no adhesion to a non-coated (PBS treated) surface (Figure 1F).
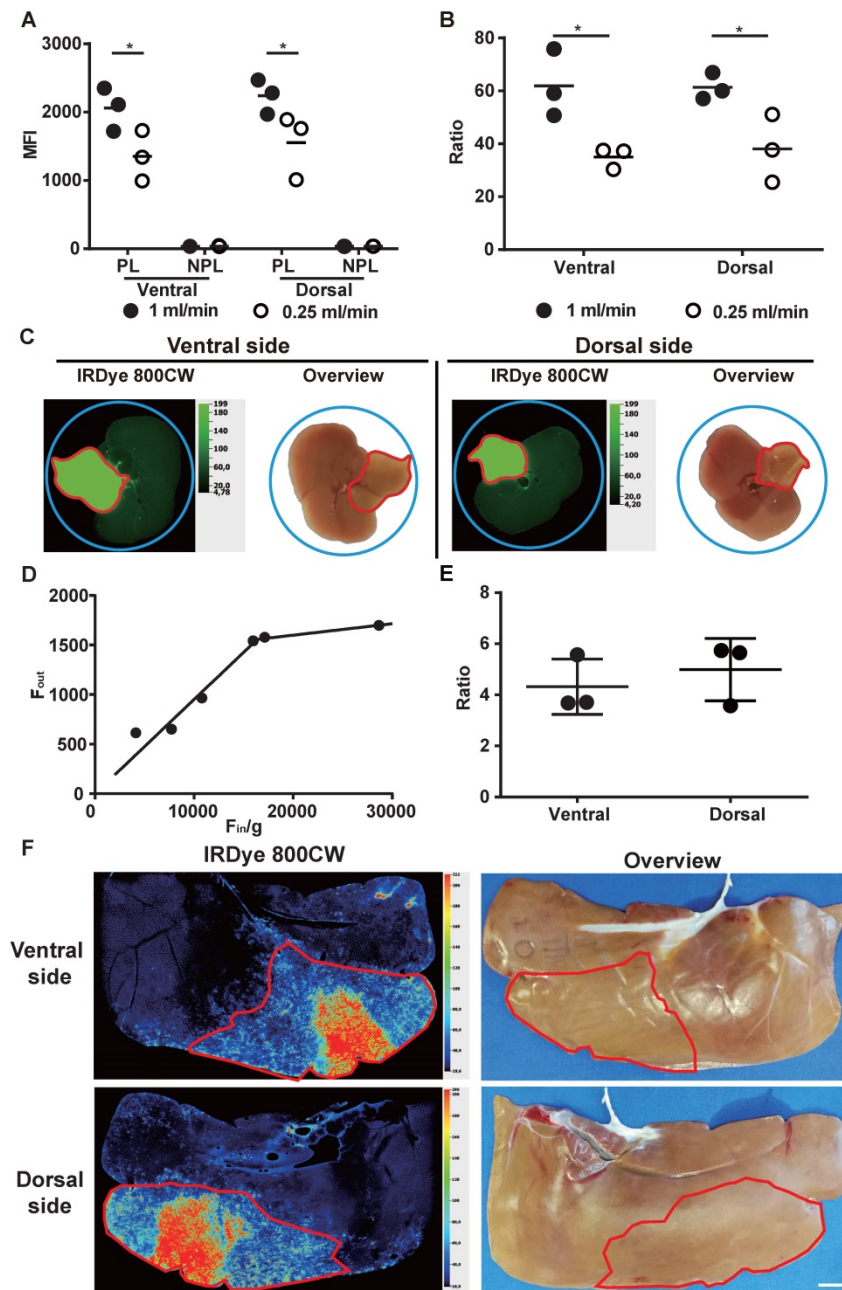

Figure 2. The efficiency of monocyte sequestration in the liver microvasculature. (A) Images showing monocyte sequestration after each 9 cycles of perfusion. Scale bar: 50 μm. (B) The monocyte sequestration efficiency. Data are presented as means ± SDs for three independent experiments. (C) Monocytes sequestration in the indicated organs at the microscopic level after selective hepatic artery injection into Panc02 tumor-bearing mice *in vivo* (n=2). The vessels were labeled with RPE –conjugated ME-9F1 mAb (orange) and monocytes were labeled with calcein (green): a, the tumor boundary; b, the perfused liver boundary; c, monocytes sequestered in the lung; d, monocytes sequestered in the pancreas; e, monocytes sequestered in the spleen; f, monocytes sequestered in the kidney. NPL: non-perfused liver; PL: peritumoral liver; T: tumor. Scale bar: 500 μm.

Monocyte sequestration *ex vivo* and *in vivo*

In order to evaluate the efficiency of monocyte sequestration in vessels, each isolated mouse liver was perfused with RPE-conjugated ME-9F1 mAb for microscopic labeling and visualization of the complete microvascular tree. Subsequently, the isolated liver was perfused with calcein-AM labeled monocytes. Fluorescence microscopy showed that the labeled monocytes were effectively sequestered in the portal area of the liver. The number of sequestered cells gradually increased in parallel with the number of perfused monocytes (Figure 2A). The efficiency of sequestration was approximately 90% and was independent of the number of perfused cells (Figure 2B). Furthermore, monocytes were almost sequestered in peritumoral liver tissue after selective hepatic artery injection in tumor-bearing mice *in vivo* . Very few monocytes were sequestered in the lung, pancreas, or spleen capillaries (Figure 2C).
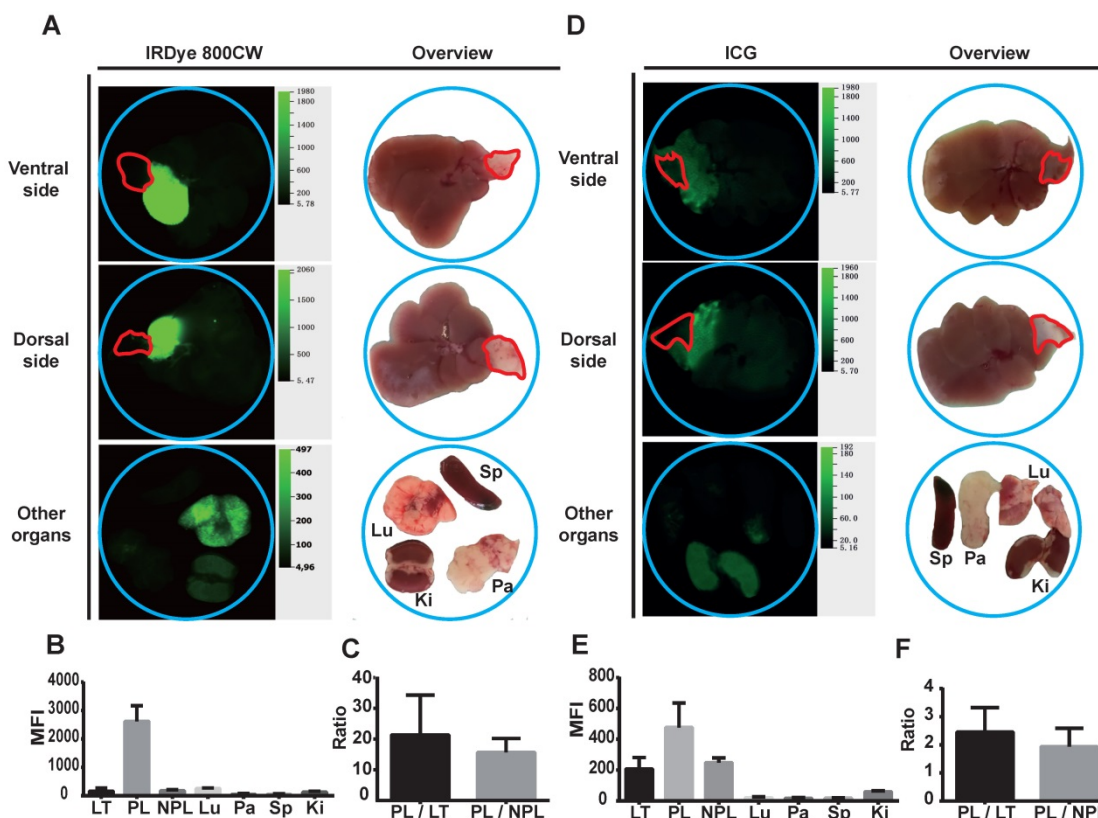

Figure 3. Liver segment labeling and visualization using IRDye 800CW-labeled monocytes ex vivo. (A–D) Liver segment labeling and visualization after perfusion of an isolated mouse liver with IRDye 800CW-labeled monocytes. (A) The mean fluorescence intensity (MFI) of perfused and control areas. (B) The fluorescence ratios. (C) Images. (D) The relationship of the injected fluorescence (Fin/g) and the obtained fluorescence (Fout) at 0.25 mL/min. (E, F) Liver segment labeling and visualization in an isolated pig liver. (E) The fluorescence ratio, and (F) images at a perfusion rate of 1 mL/min. Scale bar: 1 cm. Data are presented as means ± SDs for three independent experiments. The red line delineates the perfused liver area. NPL: non-perfused liver; PL: perfused liver. Mixed ANOVA followed by a Bonferroni correction test was used for the analysis in (A), and the t-test was used for the analysis in (B). *P < 0.05.

Excellent liver segment labeling and visualization using IRDye 800CW-labeled monocytes *ex vivo*
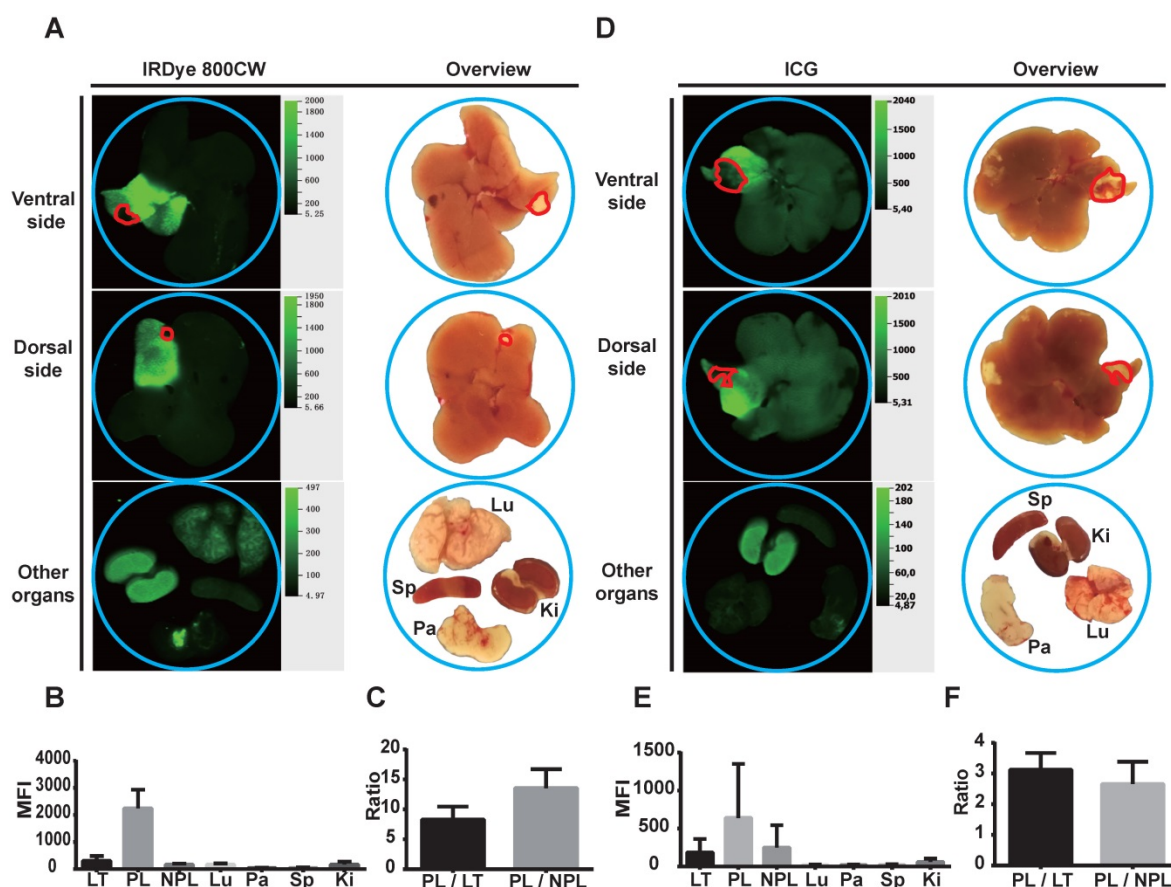
To investigate the use of labelled monocytes for the macroscopic imaging, selected mouse and pig liver segments were *ex vivo* perfused with IRDye 800CW-labeled monocytes. The result was excellent fluorescence labeling and macroscopic visualization of these segments (Figure 3C, 3F). The segments and their boundaries contrasted sharply with the non-perfused liver (Figure 3B, 3E). As the perfused cells per gram (n/g) increased, meaning that the injected fluorescence (F_{in}/g) increased, higher fluorescence (F_{out}) was obtained using a 0.25 mL/min rate. However, when the injected fluorescence was 16,000 MFI/g (approximately 1.5×10^6 monocytes/g) or more, the obtained fluorescence did not change too much (Figure 3D). The relative number of perfused cells (n/g) was higher in mouse liver than in pig liver, and this was reflected by higher imaging contrast (Figure 3B, 3E). Use of a higher perfusion rate (1 mL/min) significantly increased the fluorescence and the contrast of the segment labeling ($P < 0.05$; Figure 3A-B). The fluorescence of labeled segment was stable during 5 hours of continuous perfusion of mouse liver (Figure S2).

Perfusion of IRDye 800CW-labeled monocytes into tumor-bearing mice results in high contrast liver segments *in vivo*

To evaluate the efficiency of liver segment demarcation, locoregional injection of IRDye 800CW-labeled monocytes was performed in tumor-bearing mice and compared with ICG application. The results were analyzed using macroscopic NIR-imaging. Notably, tumor-bearing liver segments showed very strong accumulation of IRDye 800CW fluorescence. The boundaries of these segments were sharply delineated. In contrast to the labeled liver segments, the tumors did not accumulate fluorescence signal in both the Panc02 and Hep55.1C models (Figure 4A-B; 5A-B). Other organs, including lung, pancreas, spleen, and kidney, did not show a high accumulation of IRDye 800CW fluorescence (Figure 4A-B; 5A-B). ICG injection also fluorescently labeled the injected liver segment (Figure 4D-E; 5D-E). However, the signal intensity ratio after monocyte injection (a peritumoral liver-to-non-perfused liver ratio > 10) (Figure 4C; 5C) was significantly higher than the ratio after the injection of ICG (a peritumoral liver-to-non-perfused liver ratio < 2.5) ($P<0.01$) (Figure 4F; 5F).

Figure 4. Liver segment contrast in Panc02 tumor-bearing mice *in vivo* . (A–C) Liver segment contrast using IRDye 800CW-labeled monocytes. (A) Images and (B) the mean fluorescent intensity (MFI) of the indicated organs. (C) The PL/LT and PL/NPL ratios. (E–G) Liver segment contrast using ICG. (E) Images and (F) the MFI of the indicated organs. (G) The PL/LT and PL/NPL ratios. Data are presented as means ± SDs for three independent experiments. The red line delineates the liver tumor. Ki: kidney; LT: liver tumor; Lu: lung; NPL: non-perfused liver; Pa: pancreas; PL: peritumoral liver; Sp: spleen.

Figure 5. Liver segment contrast in Hep55.1C tumor-bearing mice *in vivo*. (A–C) Liver segment contrast using IRDye 800CW-labeled monocytes. (A) Images and (B) the mean fluorescent intensity (MFI) of the indicated organs. (C) The PL/LT and PL/NPL ratios. (E–G) Liver segment contrast using ICG. (E) Images and (F) the MFI of the indicated organs. (G) The PL/LT and PL/NPL ratios. Data are presented as means ± SDs for three independent experiments. The red line delineates the liver tumor. Ki: kidney; LT: liver tumor; Lu: lung; NPL: non-perfused liver; Pa: pancreas; PL: peritumoral liver; Sp: spleen.

Discussion

This study quantitatively analyzed monocyte sequestration in the liver microvascular system after hepatic locoregional application of fluorescently labeled monocytes. Most experiments used a standard flow rate of 1 mL/min, which corresponds to a physiological intraportal pressure of 10 mmHg [24]. When the liver was perfused with monocytes (1×10^6 cells/mL) at a level that was the approximately 5-fold higher than the normal monocyte count in mouse blood [26, 27], almost 90% of perfused monocytes were sequestered in the microvascular system. Indeed, monocytes were efficiently sequestered in both mouse and pig livers. Only a small fraction of monocytes (< 10%) passed through the liver and were sequestered in capillaries in other organs.

Monocytes were in direct contact with a synthetic surface during the experimental procedure but were not specifically treated or activated; nonetheless, this extracorporeal contact resulted in monocytes activation [28, 29]. Using microfluidic methods, the extracorporeal human monocytes strongly adhered to autologous ICAM-1 and to mouse

ICAM-1 even without additional treatment. Also the diameter of the monocytes is greater than the diameter of microvascular blood vessels in normal liver (Figure S1C). Both factors strongly promote monocyte sequestration in the liver microvasculature. In contrast to vessels in normal liver, the diameter of the smallest tumor-associated blood vessels was greater than the diameter of the monocytes (Figure S1C). Therefore, there was very low fluorescence contrast and very little sequestration observed in the experimental liver tumors in the present study.

The highly effective sequestration of single monocyte could be visualized at the microscopic level. Interestingly, the number of injected monocytes correlated well with the continuous increase in intravascular monocyte accumulation and with the subsequent increase in fluorescence in the liver segment. The maximum number of cells, 9×10^6 cells (approximately 6–7×10^6 cells/g), resulted in almost complete intraluminal filling of the microvascular blood vessels with monocytes. It seems likely that a further increase in the number of monocytes would exceed the volume of microvascular tree and might have negative effects on the main blood vessels, such

as thrombosis. From a translational point of view, it will be critical to determine the maximum number to avoid these negative effects. Our data suggest that this limit may be on the order of 6–7 × 10^6 cells/g.

We found that monocytes can be labeled with NIR dye using a labeled antibody or antibody cocktail. In this case, the limited antibody-specific antigens are used for conjugation/labeling. In contrast to the use of antibody labeling, direct co-incubation of cells with IRDye 800CW NHS ester uses all of the available amino groups of the cell surface proteins for conjugation, resulting in the highest degree of fluorescent labeling. Our data showed that this conjugation method did not have any cytotoxic effects. IRDye 800CW is emerging as an important NIR fluorescent dye, and it is widely used in clinical imaging. A number of antibody-IRDye 800CW conjugates are currently being tested in clinical trials. Compared with ICG, IRDye 800CW shows stable fluorescence after protein conjugation to monocytes. This made it the possible to create stable lesion-to-background contrast in the livers during the long-time perfusion. Previous studies have used IRDye 800CW-conjugated antibodies to target specific cancers. For example, cetuximab-IRDye 800CW has been used to target head and neck cancer [30] and bevacizumab-IRDye 800CW has been used to target primary breast cancer [31].

In the isolated liver perfusion experiments described here, even a low number of IRDye 800CW-labeled monocytes resulted in good liver segment labeling and contrast. We found that 1.5–2 × 10^6 cells/g was an appropriate dose for demarcating a selected segment using IRDye 800CW-labeled monocytes. Although non-conjugated IRDye 800CW and ICG have comparable molar extinction coefficients [32, 33], IRDye800CW-conjugated antibodies and proteins have substantially higher fluorescence quantum yields than ICG-conjugated [34, 35]. Therefore, IRDye 800CW may be alternative to currently approved clinical fluorescent dyes for fluorescence-guided surgery. Furthermore, superselective ICG injection, the current method for intraoperative NIR-based navigation, does not prevent ICG circulation in the peripheral blood. Because ICG is metabolized intrahepatically [36], it accumulates in the liver. These result in a continuous decrease and eventual loss of imaging contrast [10, 13]. In contrast to ICG, superselective monocyte injection leads to the almost complete sequestration of monocytes in the liver and prevents the fluorescent substance from entering the circulation. This may increase imaging contrast and improve contrast stability. In regard to invasiveness, the blood sample collected for monocyte isolation is the main difference

compared to ICG injection. The current cost of monocyte labeling for one superselective injection into human liver is $60 to $200, which is more expensive than ICG. However, clinical approval and wider use of IRDye 800CW will substantially decrease its cost. As described above, the surgeon must be well trained in ultrasound technique for the superselective injection of ICG. This issue is also important for injection of IRDye 800CW-labeled monocytes.

The experimental results of the present study provide a rationale for using superselective monocyte injection as an additional tool for liver segment labeling that can increase and probably prolong imaging contrast if needed. It can also be proposed as alternative for ICG when ICG use is not feasible. It could be important, for example, for patients with iodine allergy, although the number of such candidates is very low [16]. The potential clinical implications are mainly in fluorescence-guided navigation during parenchyma-sparing liver resection. This is a highly demanding surgical technique that aims to save as much normal liver tissue as possible and that provides a better clinical outcome [37-39]. Parenchyma-sparing liver resection is used mainly in liver tumor surgery and is strongly dependent on the exact determination of liver segment anatomy using ultrasound or/and imaging navigation [39].

Interestingly, the diameter of blood vessels in experimental tumors is significantly greater than the diameter of normal liver blood vessels and greater than the diameter of monocyte, which most likely accounts for the low level of monocyte sequestration in tumor-associated blood vessels. The tumor thus has a negative appearance on the fluorescence image, which could provide additional helpful information about tumor localization. Human liver tumors are more heterogeneous than mouse tumor models, and some human liver tumors have blood vessels with small, capillary-like diameters [40]; thus, they may also exhibit monocyte sequestration.

To summarize, the present experimental study shows that the superselective injection of isolated monocytes results in their sequestration in the hepatic microvascular system and in the demarcation of related liver segments. This technique can be used for fluorescent imaging of liver segments and may be useful for fluorescence-guided liver surgery.

Abbreviations

ICG: indocyanine green; ICAM-1: Intercellular Adhesion Molecule 1 mAb: monoclonal antiboady; MFI: mean fluorescence intensity; NHS: N-Hydroxysuccinimide; NIR: near-infrared; PBMCs: peripheral blood mononuclear cells; PBS:

phosphate-buffered saline; RPE: R-phycoerythrin.

Supplementary Material

Supplementary figures.

http://www.thno.org/v08p6101s1.pdf

Acknowledgments

Competing Interests

The authors have declared that no competing interest exists.

References

1. Garden OJ, Rees M, Poston GJ, Mirza D, Saunders M, Ledermann J, et al. Guidelines for resection of colorectal cancer liver metastases. Gut. 2006; 55 Suppl 3: iii1-8.
2. Montagnani F, Crivelli F, Aprile G, Vivaldi C, Pecora I, De Vivo R, et al. Long-term survival after liver metastasectomy in gastric cancer: Systematic review and meta-analysis of prognostic factors. Cancer Treat Rev. 2018; 69: 11-20.
3. Majno P, Mentha G, Toso C, Morel P, Peitgen HO, Fasel JH. Anatomy of the liver: an outline with three levels of complexity--a further step towards tailored territorial liver resections. J Hepatol. 2014; 60: 654-62.
4. Clavien PA, Petrowsky H, DeOliveira ML, Graf R. Strategies for safer liver surgery and partial liver transplantation. N Engl J Med. 2007; 356: 1545-59.
5. Beller S, Hunerbein M, Eulenstein S, Lange T, Schlag PM. Feasibility of navigated resection of liver tumors using multiplanar visualization of intraoperative 3-dimensional ultrasound data. Ann Surg. 2007; 246: 288-94.
6. Makuuchi M, Hasegawa H, Yamazaki S. Ultrasonically guided subsegmentectomy. Surg Gynecol Obstet. 1985; 161: 346-50.
7. Takamoto T, Hashimoto T, Ogata S, Inoue K, Maruyama Y, Miyazaki A, et al. Planning of anatomical liver segmentectomy and subsegmentectomy with 3-dimensional simulation software. Am J Surg. 2013; 206: 530-8.
8. Vahrmeijer AL, Hutteman M, van der Vorst JR, van de Velde CJH, Frangioni JV. Image-guided cancer surgery using near-infrared fluorescence. Nat Rev Clin Oncol. 2013; 10: 507-18.
9. Marshall MV, Rasmussen JC, Tan IC, Aldrich MB, Adams KE, Wang X, et al. Near-Infrared Fluorescence Imaging in Humans with Indocyanine Green: A Review and Update. Open Surg Oncol J. 2010; 2: 12-25.
10. Miyata A, Ishizawa T, Tani K, Shimizu A, Kaneko J, Aoki T, et al. Reappraisal of a Dye-Staining Technique for Anatomic Hepatectomy by the Concomitant Use of Indocyanine Green Fluorescence Imaging. J Am Coll Surg. 2015; 221: e27-36.
11. Kawaguchi Y, Ishizawa T, Miyata Y, Yamashita S, Masuda K, Satou S, et al. Portal uptake function in veno-occlusive regions evaluated by real-time fluorescent imaging using indocyanine green. J Hepatol. 2013; 58: 247-53.
12. Aoki T, Murakami M, Yasuda D, Shimizu Y, Kusano T, Matsuda K, et al. Intraoperative fluorescent imaging using indocyanine green for liver mapping and cholangiography. J Hepatobiliary Pancreat Sci. 2010; 17: 590-4.
13. Aoki T, Yasuda D, Shimizu Y, Odaira M, Niiya T, Kusano T, et al. Image-guided liver mapping using fluorescence navigation system with indocyanine green for anatomical hepatic resection. World J Surg. 2008; 32: 1763-7.
14. Kobayashi Y, Kawaguchi Y, Kobayashi K, Mori K, Arita J, Sakamoto Y, et al. Portal vein territory identification using indocyanine green fluorescence imaging: Technical details and short-term outcomes. J Surg Oncol. 2017; 116: 921-31.
15. Majlesara A, Golriz M, Hafezi M, Saffari A, Stenau E, Maier-Hein L, et al. Indocyanine green fluorescence imaging in hepatobiliary surgery. Photodiagnosis Photodyn Ther. 2017; 17: 208-15.
16. Speich R, Saesseli B, Hoffmann U, Neftel KA, Reichen J. Anaphylactoid reactions after indocyanine-green administration. Ann Intern Med. 1988; 109: 345-6.
17. Downey GP, Doherty DE, Schwab B, 3rd, Elson EL, Henson PM, Worthen GS. Retention of leukocytes in capillaries: role of cell size and deformability. J Appl Physiol. 1990; 69: 1767-78.
18. Takeishi N, Imai Y, Ishida S, Omori T, Kamm RD, Ishikawa T. Cell adhesion during bullet motion in capillaries. Am J Physiol Heart Circ Physiol. 2016; 311: H395-403.
19. Ley K, Laudanna C, Cybulsky MI, Nourshargh S. Getting to the site of inflammation: the leukocyte adhesion cascade updated. Nat Rev Immunol. 2007; 7: 678-89.
20. Nourshargh S, Alon R. Leukocyte Migration into Inflamed Tissues. Immunity. 2014; 41: 694-707.
21. Doerschuk CM. Mechanisms of leukocyte sequestration in inflamed lungs. Microcirculation. 2001; 8: 71-88.
22. Ryschich E, Kerkadze V, Deduchovas O, Salnikova O, Parseliunas A, Marten A, et al. Intracapillary leucocyte accumulation as a novel antihaemorrhagic mechanism in acute pancreatitis in mice. Gut. 2009; 58: 1508-16.
23. Phillipson M, Heit B, Colarusso P, Liu L, Ballantyne CM, Kubes P. Intraluminal crawling of neutrophils to emigration sites: a molecularly distinct process from adhesion in the recruitment cascade. J Exp Med. 2006; 203: 2569-75.
24. Winkler N, Strubing F, Gross W, Mier W, Ryschich E. Phenomenon of endothelial antibody capture: Principles and potential for locoregional targeting of hepatic tumors. Hepatology. 2018; [Epub ahead of print].
25. Bessems M, Doorschodt BM, Dinant S, de Graaf W, van Gulik TM. Machine perfusion preservation of the pig liver using a new preservation solution, polysol. Transplant Proc. 2006; 38: 1238-42.
26. Dutta P, Nahrendorf M. Regulation and consequences of monocytosis. Immunol Rev. 2014; 262: 167-78.
27. O'Connell KE, Mikkola AM, Stepanek AM, Vernet A, Hall CD, Sun CC, et al. Practical murine hematopathology: a comparative review and implications for research. Comp Med. 2015; 65: 96-113.
28. Sato Y, Hiramatsu Y, Homma S, Sato M, Sato S, Endo S, et al. Phosphodiesterase type 4 inhibitor rolipram inhibits activation of monocytes during extracorporeal circulation. J Thorac Cardiovasc Surg. 2005; 130: 346-50.
29. Johnson D, Thomson D, Hurst T, Prasad K, Wilson T, Murphy F, et al. Neutrophil-Mediated Acute Lung Injury after Extracorporeal Perfusion. J Thorac Cardiovasc Surg. 1994; 107: 1193-202.
30. Rosenthal EL, Warram JM, de Boer E, Chung TK, Korb ML, Brandwein-Gensler M, et al. Safety and Tumor Specificity of Cetuximab-IRDye800 for Surgical Navigation in Head and Neck Cancer. Clin Cancer Res. 2015; 21: 3658-66.
31. Lamberts LE, Koch M, de Jong JS, Adams ALL, Glatz J, Kranendonk MEG, et al. Tumor-Specific Uptake of Fluorescent Bevacizumab-IRDye800CW Microdosing in Patients with Primary Breast Cancer: A Phase I Feasibility Study. Clin Cancer Res. 2017; 23: 2730-41.
32. Landsman ML, Kwant G, Mook GA, Zijlstra WG. Light-absorbing properties, stability, and spectral stabilization of indocyanine green. J Appl Physiol. 1976; 40: 575-83.
33. Leung K. IRDye 800CW-Human serum albumin. Molecular Imaging and Contrast Agent Database (MICAD). Bethesda USA: National Center for Biotechnology Information; 2004.
34. Li ML, Oh JT, Xie XY, Ku G, Wang W, Li C, et al. Simultaneous molecular and hypoxia imaging of brain tumors *in vivo* using spectroscopic photoacoustic tomography. Proc IEEE. 2008; 96: 481-9.
35. Ogawa M, Kosaka N, Choyke PL, Kobayashi H. *In vivo* Molecular Imaging of Cancer with a Quenching Near-Infrared Fluorescent Probe Using Conjugates of Monoclonal Antibodies and Indocyanine Green. Cancer Res. 2009; 69: 1268-72.
36. Leevy CM, Smith F, Longueville J, Paumgartner G, Howard MM. Indocyanine Green Clearance as a Test for Hepatic Function. JAMA. 1967; 200: 236-40.
37. Aghayan DL, Pelanis E, Avdem Fretland A, Kazaryan AM, Sahakyan MA, Rosok BI, et al. Laparoscopic Parenchyma-sparing Liver Resection for Colorectal Metastases. Radiol Oncol. 2018; 52: 36-41.
38. Moris D, Dimitroulis D, Vernadakis S, Papalampros A, Spartalis E, Petrou A, et al. Parenchymal-sparing Hepatectomy as the New Doctrine in the Treatment of Liver-metastatic Colorectal Disease: Beyond Oncological Outcomes. Anticancer Res. 2017; 37: 9-14.
39. Alvarez FA, Sanchez Claria R, Oggero S, de Santibanes E. Parenchymal-sparing liver surgery in patients with colorectal carcinoma liver metastases. World J Gastrointest Surg. 2016; 8: 407-23.
40. Chen ZY, Wei W, Guo ZX, Lin JR, Shi M, Guo RP. Morphologic classification of microvessels in hepatocellular carcinoma is associated with the prognosis after resection. J Gastroenterol Hepatol. 2011; 26: 866-74.